Spontaneous Raman Scattering Spectroscopy of a Resistojet Plume in a Vacuum Environment

IEPC-2017-544

Presented at the 35th International Electric Propulsion Conference
Georgia Institute of Technology – Atlanta, Georgia – USA
October 8–12, 2017

Alfredo D. Tuesta *
and Brian T. Fisher †
Chemistry Division, Naval Research Laboratory, Washington DC, 20375

and

Joel A. Silver ‡
Southwest Sciences, Inc., Santa Fe, NM 87505

and

Logan T. Williams §
and Michael F. Osborn ¶
Spacecraft Engineering Department, Naval Research Laboratory, Washington DC, 20375

With the increasing interest in the use of nanosatellites, such as CubeSats, to perform scientific research in space and conduct Earth observation and communications, efficient designs for propulsion systems are necessary. Resistojests are being studied for this purpose and current modeling efforts to optimize nozzle design require experimental validation. In this report, the design for a low pressure, highly spatially resolved spontaneous Raman scattering spectroscopy system is developed and tested in a gas cell with ambient N_2 and O_2. This novel approach shows that gains may be achieved with a multiple-pass cell, EMCCD camera and holographic spectrograph using a probe volume of approximately 100-μm in diameter and 172-μm long. The system will be used to study the temperature and number density in the plume of a resistojet in the mTorr pressure range.

*Performed the work as a National Research Council Postdoctoral Associate at the Naval Research Laboratory.
†Research Mechanical Engineer. Corresponding author: brian.fisher@nrl.navy.mil.
‡Executive Vice President, Southwest Sciences.
§Research Aerospace Engineer.
¶Section Head, Propulsion Section.

Nomenclature

f	= final state
i	= initial state
J	= rotational quantum number
l	= length of beam segment
n_0	= molecular number density
N_L	= number of incident photons
$N_{i\rightarrow f}$	= number of photons scattered
$\frac{n_i}{n_0}$	= population fraction in the initial state
P	= gas pressure
R	= reflectivity of mirror
ν	= vibrational quantum number
$d\Omega$	= solid angle
$\left(\frac{d\sigma}{d\Omega}\right)_{i\rightarrow f}$	= differential Raman cross section

I. Introduction

Since the late 1950s, pico- and nanosatellites have been launched into space in an effort to extend man's reach into the universe and to perform scientific experiments.[1] These low cost, lightweight CubeStats are attractive to research centers and universities for their ability to carry high-tech instruments to outer space and perform research from a unique perspective. Current propulsion mechanisms limit the lifetime of CubeStats, however, and studies have shown that resistojets have the potential to significantly extend their utility while in orbit.[2,3] At the US Naval Research Laboratory (NRL) in Washington DC, resistojets are studied for an optimal design by exploring various nozzle geometries, flow rates and propellent composition.[4]

One of the main challenges in the design of micro-resistojets is the viscous and heat transfer losses resulting from the low Reynolds regime in which these instruments operate. The small length scales in these nozzles along with the changes in viscosity of the propellant with temperature make resistojets susceptible to these type of losses.[5] Modeling efforts to explain and predict the physics in nozzle plumes are vital to improve these designs.[5–7] Experiments to validate the performance of various designs have been performed as well. For instance, the thrust and specific impulse of micro-resistojets have been measured.[2,4,8] However, *in situ* measurements of the temperature, velocity, and number densities in the plume are more difficult. The small length scales require measurements with high spatial resolution and the low pressures necessitate techniques with high sensitivity. Using probes in the flow would not provide the spatial resolution required and would adversely affect the flow itself.[9] Together, these obstacles result in a difficult but interesting diagnostic challenge.

Optical spectroscopy is a well established field capable of addressing these obstacles. Because of its high spatial resolution and signal strength, coherent anti-Stokes Raman scattering (CARS) spectroscopy has been used to probe resistojets plumes.[7,10] The velocity and translational temperature of H_2 inside and outside the nozzle was measured. CARS, however, is an expensive, complicated technique requiring at least two lasers, many optics and ample laboratory space to prepare and align the beams to the probe volume. Spontaneous Raman spectroscopy (SRS), on the other hand, is a much simpler approach requiring one laser beam, fewer optics and less space. Like CARS, SRS is capable of measuring the temperature and number density of diatomic gases in a flow from the shape and intensity of the Raman shifted spectrum.[11–16] Its main disadvantage over CARS, however, is the much weaker Raman signal that it yields. CARS is a four-wave mixing technique in which two photons stimulate the Raman polarization of the molecule and a third photon scatters resulting in a coherent, fourth photon – the Raman shifted signal. This stimulated approach results in a much stronger signal over the spontaneous approach.

Because it is proportional to the incident photon energy, there are techniques available to amplify the Raman signal. Increasing the photon influx at the probe volume may be accomplished by increasing the laser energy output or by increasing the number of beam passes through the probe volume. High energy beams, however, often require large and expensive instruments. The latter of the two techniques can be a much simpler and inexpensive approach. Multiple-pass cells or modified Herriott cells have been used for

this purpose since the 1970s.[17–19] More recent adaptations have accomplished high gains in the signal-to-noise ratio of up to 83 with 100 passes over the single pass approach with relatively high spatial resolution using a probe region of 200-μm by 300-μm at atmospheric conditions.[20,21] To the authors' knowledge, these techniques have not been implemented at the mTorr pressure range necessary to study resistojet plumes.

In this paper, the authors present a technique for highly spatially resolved, low pressure SRS to be implemented in the viscous resistojet plume to measure temperature and number density. Although similar to previous efforts, the multiple-pass cell is a unique design that allows more highly spatially resolved measurements to be performed. A high energy, continuous wave (CW) laser and state-of-the-art holographic spectrograph will be used to push the limits of low pressure SRS.

Although the performance of the resitojet needs to be studied under conditions with a variety of gas propellants, the vibrational modes are not expected to be populated at the low pressures of interest. Therefore, the rotational modes will be probed. Although the preliminary results reported in this paper are limited to benchtop measurements with ambient nitrogen and oxygen that include both rotational and vibrational modes, near future work will study the rotational temperature and number density of H_2, initially in a gas cell for calibration followed by measurements of the resistojet plume.

II. Theory

The theory of Raman scattering has been extensively described elsewhere[11,16] and is only briefly outlined here. Raman scattering is an inelastic, linear, two-photon scattering event in which the incident photon causes a change in the molecular quantum state of a molecule, thus resulting in a change in energy of the photon. The rotational and vibrational states of the molecule predominantly play a role. For a diatomic, the selection rules are $\Delta J = 0, \pm 2$ and $\Delta\nu = 0, \pm 1$ where J is the rotational quantum number, ν is the vibrational quantum number, $\Delta J = J_f - J_i$ and $\Delta\nu = \nu_f - \nu_i$.[11,12] The case in which $\Delta J = 0$ and $\Delta\nu = 0$ is known as Rayleigh scattering, an elastic scattering event. The following table summarizes the designation at each rotational and vibrational selection rule.

Table 1. Designation for rotational and vibrational selection rules.

Selection Rule		Designation
$\Delta J = 0,$	$\Delta\nu = 0$	Rayleigh scattering
$\Delta J = \pm 2,$	$\Delta\nu = 0$	pure rotational, Raman scattering
$\Delta J = 0,$	$\Delta\nu = \pm 1$	pure vibrational, Raman scattering
$\Delta J = \pm 2,$	$\Delta\nu = \pm 1$	rovibrational, Raman scattering

In a gas at thermal equilibrium, the Boltzmann distribution describes the spread of molecules across all possible rotational and vibrational states. When the excitation source for the scattering process is a single-frequency laser, many lines appear in the spectrum shifted from the incident photons, and this can be modeled for a given molecule and temperature. Each molecule has a unique spectral signature as a result of their rotational-vibrational coupling constants. Furthermore, as temperatures increases, higher rotational states are populated. The vibrational band appears to broaden in the spectrum. Depending on the resolution of the spectrograph, the rotational lines may be resolved, permitting more easily the acquisition of the rotational temperature by use of a theoretical model. At high temperatures, a secondary and tertiary vibrational band known as hot bands may appear in the spectrum, permitting the acquisition of the vibrational temperature. In thermal equilibrium, of course, these temperatures are the same. However, it is unlikely that the rotational and vibrational modes will be in equilibrium because of the supersonic gas expansion through the nozzle.

The number of photons scattered, $N_{i\to f}$, during the Raman effect and collected from a solid angle $d\Omega$ through a beam segment of length l is given by

$$N_{i\to f} = N_L l n_0 \frac{n_i}{n_o} \left(\frac{d\sigma}{d\Omega}\right)_{i\to f} d\Omega \tag{1}$$

where N_L is the incident number of photons from the laser beam, n_0 is the molecular number density, $\frac{n_i}{n_0}$ is the population fraction in the initial state, and $\left(\frac{d\sigma}{d\Omega}\right)_{i\to f}$ is the differential Raman cross section for the

transition $i \rightarrow f$.

The Raman effect is a weak process, orders of magnitude lower than Rayleigh scattering. Furthermore, the signal scales with pressure, P. Although the term is not included in Equation 1, the pressure term is folded into the molecular number density, n_0, and is directly proportional to it. Consequently, at the pressures of interest in this project, < 1 Torr, the Raman signal will be severely attenuated.

Unlike other scattering events, the direction of highest intensity of Raman scattering depends on the orientation of the incident beam. This corresponds to a solid angle of Raman photons, $d\Omega$, orthogonal to the laser beam. This means that the intensity of the Raman signal can be amplified, although to a limit, by increasing the aperture window collecting the signal.

III. Experimental Methods

A. Collecting Optics

The goal of the collecting optics is to collect as many of the Raman photons in the solid angle emanating at a right angle from the beam envelope inside the optical cavity while also controlling the diameter of the probe volume. The probe volume is defined by the volume in space irradiated by the laser beam and the section of this volume that is viewed from the collecting optics. This topic is elaborated in Section III B.

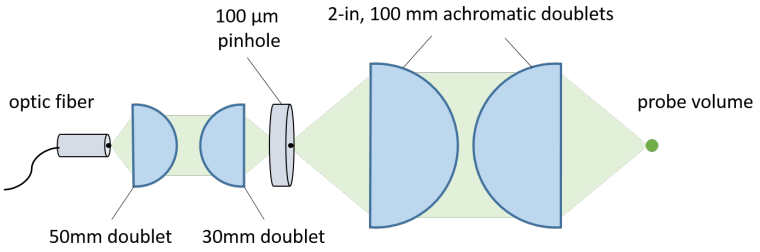

Figure 1. Optical setup of collection optics. Optics are mounted on a cage system.

Two achromatic, doublet lenses of 100-mm focusing length and 2-inch in diameter (Thorlabs, AC508-100-A) are used to collect the solid angle and refocus the Raman photons to a pinhole, as shown in Figure 1. The pinhole acts as the entrance window to the collecting optics and limits the diameter from which the Raman photons are collected. In this preliminary work, a 100-μm pinhole is used.

Following the pinhole, two air-spaced, achromatic doublets are used to collimate and refocus the Raman photons into an optical fiber. The first is a 1-inch diameter doublet with 30-mm focusing length (Thorlabs, ACA254-030-532). The second is a 1-inch diameter doublet with 50-mm focusing length (Thorlabs, ACA254-050-A). The numerical aperture and diffraction limit of the Raman photons focused into the optical fiber have been considered when designing the collection optics such that they are not obstructed by any of the optics and couple with the fiber core adequately. The collection optics are fixed on a Thorlabs cage system that provides a sturdy mechanism with which each optic may be translated along the optical axis to optimize alignment.

The optical fiber, discussed in more detail below, delivers the Raman signal to a Holographic spectrograph, F/1.8, from Andor Technology (Kaiser, HOLOSPEC-F/1.8i-VIS) that separates the colors in the signal to create the Raman spectra. The grating is a holographic grating, 2455 l/mm, 532-nm optimized, Stokes side, 92.3 cm^{-1}/mm. Inside the spectrograph is a super-notch filter (Andor, HS-HSPF-532.0) centered at 532-nm with OD greater than 6 to suppress the Rayleigh signal at 532-nm and less than 350 cm^{-1} spectral bandwidth. An Andor EMCCD camera (Newton), capable of extremely low dark current (< 0.001 eles/pix/sec), 1600 pixels $\times$ 200 pixels, is used to record the spectra.

B. Multiple-pass Cell

The multiple-pass optical cell is composed of two high-reflectivity ($R > 99.7\%$), 2-inch diameter, concave mirrors of focal length 50-mm custom made by Rocky Mountain Instruments. The mirrors are mounted on high precision kinematic mounts (Thorlabs, POLARIS-K2F3) as shown in Figure 2. A small hole a few millimeters in diameter was made through one of the mirrors to allow the beam to enter and exit the

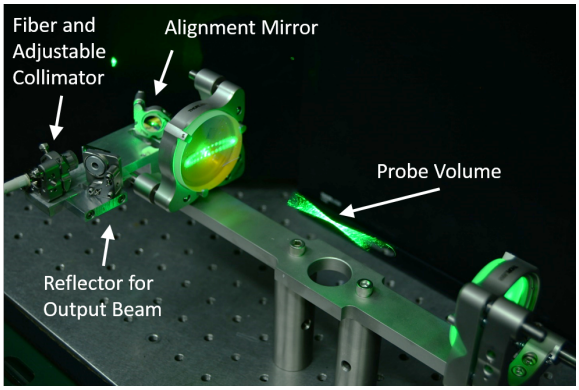

Figure 2. Multiple-pass cell showing green beam from fiber optic reflecting off of alignment mirror into optical cell. The beam reflects between the concave mirrors spaced at nearly 4x the focal length of the mirrors creating an elliptical pattern.

cell. The optical fiber delivering the 532-nm beam is mounted on a kinematic mount and focused with an adjustable collimator (Thorlabs, CFC-11X-A). An aligning mirror (Thorlabs, Y2-0525-45) is used to direct the beam into the cell through the hole. The aligning mirror is also mounted on a kinematic mount (Thorlabs, POLARIS-K05S2).

The beam is mode matched to the cell cavity and its beam waist is located between the two mirrors by adjusting the collimator such that each spot on the mirror is the same size. This results in each passing beam having the same beam waist at the probe region. The elliptical pattern formed on the surface of each mirror is similar to the envelope pattern cross section at the probe region, except that the number of passes at the probe region is twice the number of spots on the mirror. The major and minor axis of the elliptical pattern can be directly controlled by the angle at which the beam enters the optical cell. The number of passes is controlled by the spacing between the concave mirrors that form the optical cell. The primary limits to achieving a higher number of passes and a smaller envelope size are geometric restrictions. The outgoing beam must exit the optical cavity entirely and not be clipped by the edge of the hole. Also, the outgoing beam must not be reflected back into the fiber collimator, to prevent damage, as may happen with higher number of passes.

In this preliminary effort, the cell has been configured to 46 total number of passes in the cell. Once the beam has completed its trajectory in the optical cell, it exits through the same hole from where it entered at an angle from the entering beam. After exiting the optical cell, it is reflected by the alignment mirror and then by another mirror used to redirect the beam away from the fiber collimator and into a beam dump.

In Figure 2, the low energy beam can be seen forming an elliptical pattern on the mirrors. An aerosol spray is used in the area of the probe volume to visualize the converging beams. The beam can also be seen to strike the curtain in the background. At the probe volume, the beams do not fully overlap in space. For this optical cell configuration, overlapping beams would mean a maximum of two passes and the entering beam would be immediately reflected back through itself. At the top and bottom ends of the envelope, however, the beams do partially overlap which allows for a tighter probe volume, discussed below.

With the help of software specifically developed for this project by Southwest Sciences, Figure 3 illustrates the cross-section envelope at the probe volume for 46 passes. In this preliminary effort, the length of the major axis was approximately 700-μm long. This was measured by translating the collecting optics laterally across the probe volume and recording the positions where the signal decreased to zero, corresponding to the top and bottom edge of the elliptical envelope. The beam waist at the probe volume of each passing beam was measured via the knife-edge technique and estimated at 86-μm. The length of the minor axis is estimated as 2$\times$ to 3$\times$ the beam waist at the probe volume ($\sim$ 172-μm – 258-μm).

The number of passes in the elliptical envelope becomes more dense at the top and bottom ends, as illustrated in Figure 3 where they partially overlap. To maintain high spatial resolution of the measurements in this project, the pinhole limits the diameter of the probe volume (100-μm). The length of the probe volume, therefore, is defined by the width of the portion of the envelope viewed. In this preliminary work, the length is estimated at twice the beam waist (172-μm). With the illustration from the software, 4 or 6 passes through this volume are estimated out of the 46 total number of passes in the envelope. The

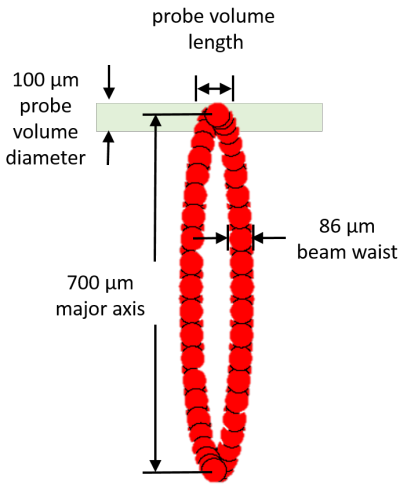

Figure 3. Cross sectional view of envelope created by multiple pass of beams near the probe volume. The diameter of the probe volume is defined by a 100-μm pinhole and its length by the width of partially overlapping beams at the top (or bottom) end of envelope.

multiple-pass cell, however, has been designed for a maximum of 100 total passes.

C. Optical Setup

Measurements of the resistojet plume are planned on a thrust stand inside NRL's South Vacuum Chamber, a chamber 2-m in diameter and 2.3-m tall, with a base pressure of 5.5×10^{-6} Torr.[2] Making scientific instruments vacuum compatible is an expensive and time consuming task. Therefore, the optical setup in this project minimizes the number of components that must be introduced into the chamber. Furthermore, because of limited optical access in this chamber, the laser light used as the excitation source in these measurements must be directed into the chamber by an optical fiber specially manufactured to withstand the high energies required. Therefore, the only items that will be introduced into the chamber are the collection optics, the multiple-pass cell, three motorized translational stages, and two optical fibers: one to deliver the high power excitation beam into the chamber, the other to deliver the Raman signal out of the chamber.

The excitation beam for these experiments come from a free space, 532-nm wavelength, CW Coherent Verdi G5 SLM laser with a waist diameter of approximately 2.2-mm and 5-W maximum power output. The optical fiber (LMA-PM-10) used to deliver the high energy beam is a single mode, polarization maintaining photonic crystal fiber from NKT Photonics with an estimated mode field diameter of 8.4-μm and a numerical aperture of 0.07. The fiber was connectorized with FC/UPC connectors on each end and adapted to the vacuum chamber by Coastal Connections. A second fiber, with numerical aperture of 0.22, is used to deliver the Raman signal out of the chamber. Both fibers pass through a vacuum feedthrough with a stainless steel tube and a $2^3/_4$-in CF flange, assembled of Coastal Connections.

To properly couple the free space beam to the fiber, a high energy beam expander (Thorlabs, BE02-532) was used to reduce the diameter of the beam from 2.2-mm to 1.1-mm and a high energy objective lens (Thorlabs, LMH-20X-532) was used to focus the beam. This fiber launch setup is illustrated in Figure 4. The numerical aperture and theoretical diffraction limit of these components were considered when designing this fiber launch system.

The collecting optics and multiple-pass cell must translate together to scan the plume because the resistojet is mounted on a thrust stand unable to translate in space. To accomplish this, a diamond shaped plate was designed on which to mount the optics as shown in Figure 5. The multiple-pass cell is fixed onto the plate. The collecting optics are mounted on a three-dimensional, vacuum compatible, compact stage (Newport, 562-XYZ V6) orthogonal to the laser beams in the multiple-pass cell. A 2-in reflector (Thorlabs, CM508-100-E02) opposite to the collecting optics is mounted on two vacuum compatible translational stages (Newport, UMR5.16V6). This reflector is a concave mirror with 100-mm focusing length that will reflect the Raman signal emitted in that direction to the collecting optics and increase the measured signal. Trans-

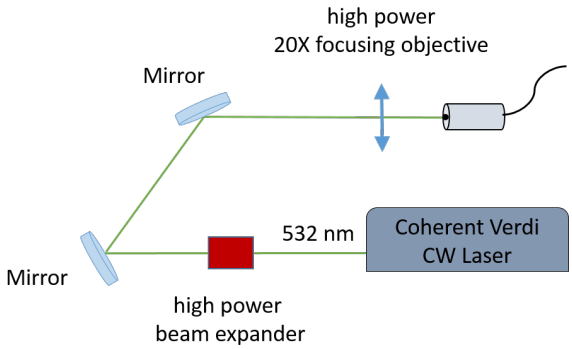

Figure 4. Fiber launch system that couples the free space beam to the optical fiber. A high power beam expander is used to reduce the beam diameter and a high energy objective lens to focus the beam.

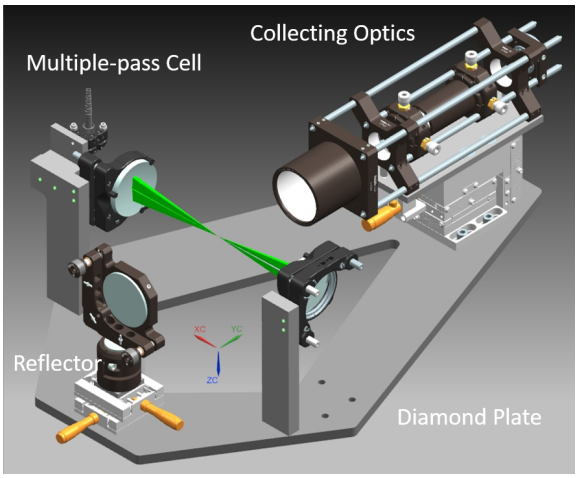

Figure 5. Optical setup of collecting optics, multiple-pass cell and reflector mounted on diamond plate for ease of translation about the resistojet in the vacuum chamber.

lation stages for the collecting optics and the reflector are needed because the exact position of the probe volume will change with the number of passes and the envelope size of the multiple-pass cell. The plate will be translated by three Velmex (MN10-0050-M01-21) stages, not shown. The resistojet is positioned at the center of the diamond plate.

The benchtop, preliminary measurements presented in this paper were conducted outside of the vacuum chamber and using a 6-way cube from LDS Vacuum Shopper (275-CUBE-OS). The cubic gas cell provides optical access for the multiple-pass cell and the collecting optics while allowing mTorr-range pressures with select gases. A rotary vane vacuum pump (Varian SD-90) is used to reduce the pressure in the cell.

IV. Results

As mentioned in the Introduction, the performance of the resistojet plume needs to be studied under a variety of conditions including an assortment of nozzle geometries and a combination of gas propellants. H_2 is an ideal gas propellant to study because its rotational lines are well spaced, allowing rotational temperature and a number density to be obtained by fitting the measured spectrum to a theoretical model. However, the number density of other diatomics, such as N_2, can also be measured with adequate calibration of the system.

To illustrate the utility of the present setup, particularly the multiple-pass cell, this preliminary work focuses on measuring N_2 and O_2 from ambient air in a cubic gas cell. The EMCCD camera exposure time was set to 1-s with an software EM gain of 150 out of 250. The laser was set to 5-W beam power but

transmission through the optical fiber and other optics was approximately 2.70-W (54% of the input).

A. Single-pass vs. Multiple-pass Approach

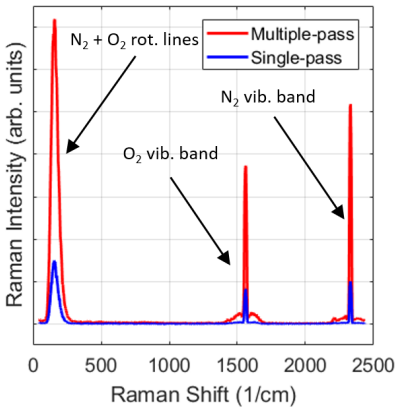

Figure 6. Gain of Raman signal from single-pass to multiple-pass approach.

Although it can be increased, the total number of passes in the envelope of the multiple-pass cell for this preliminary study was set to 46 with approximately 4 to 6 in the probe volume. To determine the gain achieved with this configuration, the Raman signal at atmospheric pressure was first measured by diverting the beam to a beam dump by placing a mirror in its path within the multiple-pass cell. Then, the mirror was removed and the beam was allowed to complete 46 passes in the cell. Spectra in single-pass and in multiple-pass approach were acquired to compare the two. Figure 6 illustrates the gain measured. The multiple-pass approach achieved a gain of approximately 4.8 in intensity, within the 4 to 6 range expected.

In future measurements, the authors expect to increase the total number of passes in the envelope close to 100, resulting in higher gains in signal.

B. Change in Pressure

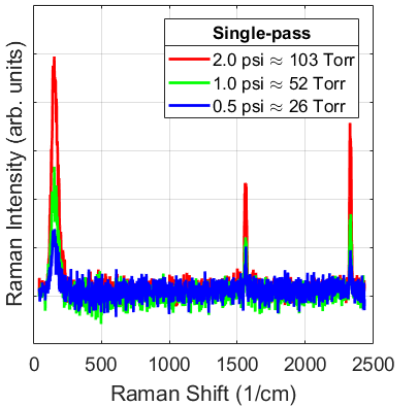

Figure 7. Decreasing pressure to determine lower limit for detectability of rotational lines in single-pass approach.

The gas cell was filled with ambient air and its pressure brought down to a few psi to test the lower limit of detectability of the rotational lines from the noise. As shown in Figure 7, at approximately 0.5 psi (26 Torr) the signal is nearly twice the noise. Pressures under 26 Torr would be more difficult to measure in the single pass approach. Also, the intensity of the Raman signal scales with pressure linearly as expected from Equation 1 when replacing n_0 with P and a scaling factor.

V. Discussion and Conclusion

The preliminary results show that the gain achieved with the multiple-pass approach is proportional to the expected number of passes in the probe volume. Furthermore, the Raman signal was seen to scale linearly and with pressure and with the camera settings utilized, a lower limit of 26 Torr was established for the N_2 and O_2 rotational lines. If the multiple-pass approach had been implemented, it is expected that the lower limit should have been reduced by about 4.8 $\times$ to $\sim$ 5 Torr. With additional number of passes, longer exposure times, and higher camera gains, the authors expect to be able to detect the rotational lines of N_2 and O_2 at pressures under 1 Torr.

Lastly, as noted previously, about 54% of the 5 W beam was transmitted through the fiber. At the low beam energies used for alignment of the fiber launch system, nearly 64% of the beam energy is transmitted. This 10% loss, if regained with better alignment at higher laser powers, could further lower the pressure limit of detectability in the system by irradiating more energy to the probe volume.

Acknowledgments

The authors thank the Office of Naval Research for supporting this work through the NRL Base Program and the National Research Council for administering the NRL postdoctoral research associateship program.

References

[1]J. Bouwmeester and J. Guo. Survey of worldwide pico- and nanosatellite missions, distributions and subsystem technology. *Acta Astronautica*, 67:854–862, 2010.

[2]Logan T. Williams and Michael F. Osborn. Performance impacts of geometry and operating conditions on a low reynolds number micro-nozzle flow. *35th International Electric Propulsion Conference*, IEPC-2017-120, 2017.

[3]M. F. Osborn, T. D. Holman, D. A. Rosenberg, S. G. Tuttle, and L. T. Williams. Overcoming low nozzle efficiency: A test correlated numerical investigation of low reynolds number micro-nozzle flow. *51st AIAA/SAE/ASEE Joint Propulsion Conference*, AIAA-2015-3925, 2015.

[4]L. T. Williams, McDonald M. S., and M. F. Osborn. Performance characterization of a low reynolds number micro-nozzle flow. *51st AIAA/SAE/ASEE Joint Propulsion Conference*, AIAA-2015-3924, 2015.

[5]Timothy D. Holman and Michael F. Osborn. Numerical optimization of micro-nozzle geometries for low reynolds number resiso-jets. *51st AIAA/SAE/ASEE Joint Propulsion Conference*, AIAA-2015-3923, 2015.

[6]Timothy D. Holman and Michael F. Osborn. On the validation of direct numerical monte carlo method for low reynolds number micro-nozzle resisto-jets. *35th International Electric Propulsion Conference*, IEPC-2017-306, 2017.

[7]I. D. Boyd, D. B. VanGilder, and E. J. Beiting. Computational and experimental investigations of rarefied flows in small nozzles. *AIAA Journal*, 34(11):2320–2326, 1996.

[8]Riki H. Lee, Taylor C. Lilly, E. P. Muntz, and Andrew D. Ketsdever. Free molecule micro-resistojet: Nanosatellite propulsion. *AIAA*, 5026, 2005.

[9]David A. Rosenberg, Bradley A. Williams, Steven G. Tuttle, and Michael F. Osborn. Optical measurements of density and species concentration in a low reynolds number micro-nozzle flow. *53rd AIAA Aerospace Sciences Meeting*, 1148, 2015.

[10]Edward J. Beiting. Coherent anti-stokes raman scattering velocity and translational temperatures measurements in resistojets. *Optical Society of America*, 36(15):3565–3576, 1997.

[11]Alan C. Eckbreth. *Laser Diagnostics for Combustion Temperature and Species*. Taylor and Francis, Berlin, 1996.

[12]D. R. Beattie and M. A Cappelli. Raman scattering measurements of molecular hydrogen in a low-density, arc-heated plasma. *Applied Physics B*, 70:419–427, 2000.

[13]George J. Williams, Jun J. Kojima, Lynn A. Arrington, Matthew C. Deans, Brian D. Reed, McKenzie I. Kinzbach, and Christopher H. McLean. Plume characterization of a laboratory model 22 n gpim thruster via high-frequency raman spectroscopy. *AIAA Join Propulsion Conference*, 3754, 2015.

[14]I. D. Boyd, D. R. Beattie, and M. A. Cappelli. Numerical and experimental investigations of low-density supersonic jets of hydrogen. *Journal of Fluid Mechanics*, 280:41–67, 1994.

[15]Wilhelmus A. de Groot and Frank J. Zupanc. Laser rayleigh and raman diagnostics for small hydrogen/oxygen rockets. *Proceedings of SPIE*, 1862:98–112, 1993.

[16]Jun Kojima and Quang-Viet Nguyen. Quantitative analysis of spectral interference of spontaneous raman scattering in high-pressure fuel-rich h_2-air combustion. *Journal of Quantitative Spectroscopy and Radiative Transfer*, 94:439–466, 2005.

[17]Jack Loader. *Basic Lasr Raman Spectroscopy*. Heyden and Son Ltd., Philadelphia, PA, 1970.

[18]A. Weber. *Raman Spectroscopy of Gases and Liquids*. Springer-Verlag, Berlin, 1979.

[19]W. R. Trutna and R. L. Byer. Multi-pass raman gain cell. *Applied Optics*, 19:301–312, 1980.

[20]Utsav K.C., Joel A. Silver, David C. Hovde, and Philip L. Varghese. Improved multiple-pass raman spectrometer. *Applied Optics*, 50(24):4805–4816, 2011.

[21]K. C. Utsav and Philip L. Varghese. Accurate temperature measurements in flames with high spatial resolution using stokes raman scattering from nitrogen in a multiple-pass cell. *Optical Society of America*, 52(20):5007–5021, 2013.